

A New Wavelet Completed Local Ternary Count (WCLTC) for Image Classification

Taha H. Rassem^{1,2}, Fatimah A. Alkareem¹, Mohammed Falah Mohammed³, Nasrin M. Makbol², and Amer Sallam⁴

¹Faculty of Computing, College of Computing and Applied Sciences, Pekan, Malaysia
Email: tahahussein@ump.edu.my

²College of Computer Science and Engineering, University of Hodeidah, Yemen.

³Computer and communication engineering, Nawroz University, Iraq

⁴Alsaeed Faculty for Engineering & IT, Taiz University, Yemen

Abstract—To overcome noise sensitivity and increase the discriminative quality of the Local Binary Pattern, a Completed Local Ternary Count (CLTC) was developed by combining the Local Ternary Pattern (LTP) with the Completed Local Binary Count (CLBC) (LBP). Furthermore, by integrating the proposed CLTC with the Redundant Discrete Wavelet Transform (RDWT) to construct a Wavelet Completed Local Ternary Count, the proposed CLTC’s discriminative property is improved (WCLTC). As a result, more accurate local texture feature capture inside the RDWT domain is possible. The proposed WCLTC is utilised to perform texture and medical image classification tasks. The WCLTC performance is evaluated using two benchmark texture datasets, CURET and Outex, as well as three medical picture databases, 2D Hela, VIRUS Texture, and BR datasets. With several of these datasets, the experimental findings demonstrate a remarkable classification accuracy. In several cases, the WCLTC performance outperformed the prior descriptions. With the 2D Hela, CURET, and Virus datasets, the WCLTC achieves the highest classification accuracy of 96.91%, 97.04 percent, and 72.89%, respectively.

I. INTRODUCTION

Recently, texture features have become more popular and important in several applications such as image classification [1], [2], face recognition [3], [4], human detector [5]. These texture features have a variety of properties that allow them to be used in a variety of situations.

Model-based methods, statistical algorithm methods, and structural methods have all been used to classify texture features [6]. The texture is generally displayed as a likelihood model of a set of major functions in model-based approaches. Kashyap [7] proposed the Circular Simultaneous Autoregressive (CSAR) model for texture invariant features. Statistical algorithm methods fall into the second category. The texture is usually categorised in this category by statistics of selected aspects like micro-structure and invariant histogram. Duvernoy [8] introduced Fourier descriptors for obtaining the rotation invariant texture feature on the spectrum field. The structural approaches, such as topological texture descriptors, are the third category. In 2002, Ojala proposed the Local Binary Pattern (LBP), which is now widely used as a texture

feature for texture classification [9]. Several image processing tasks employ the LBP descriptor, including scene and object recognition [1], human detections, object tracking [10], and face recognition. The user limit patterns (grid of cells) that are explained in full in section II are used to generate the local binary pattern histogram. Since 2002, many texture descriptors are proposed such as the Local Ternary Pattern (LTP) [11], Completed LBP (CLBP) [12], Completed Local Binary Count (CLBC) [13], and Completed Local Ternary Pattern (CLTP) [14]. Although the LBP demonstrated good reaction and performance in several areas, it had some flaws. Many texture characteristics are offered that are based on LBP and inherit its flaws. As illustrated in Figure 1 and Figure 2, the LBP is sensitive to noise, and diverse patterns of LBP can be grouped into the same class, reducing its discriminating property [12], [11]. These flaws were passed down to the CLBP and CLBC. CLTP is designed to address these flaws; nevertheless, CLTP’s bin length is significantly longer than that of prior texture descriptors. This may have an impact on its performance with certain datasets.

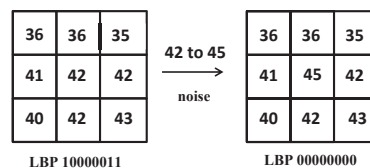


Fig. 1. Example of the LBP operator’s noise sensitivity.

The Completed Local Binary Count (CLBC) texture descriptor is given a new enhancement in this paper. To solve the sensitivity to noise drawback, the LTP is combined with CLBC to develop a new texture descriptor. In addition, the new texture is extracted in the wavelet domain rather than the spatial domain to improve the suggested descriptor’s discriminative property. Wavelet Completed Local Ternary Count is the name of the new texture descriptor (WCLTC). The proposed

90	80	100
70	20	16
10	50	3

LBP 01111010

100	200	105
102	100	90
40	130	20

LBP 01111010

Fig. 2. Example of classifying falsely problem.

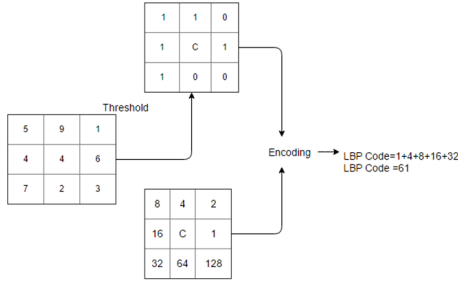


Fig. 3. The basic of Local Binary Pattern

WCLTC's performance is assessed using a variety of texture and medical image datasets.

The rest of this paper is organised as follows. The Related Works are briefly reviewed in Section II. The proposed WCLTC is presented in Section III. The experimental data and discussion are offered in Section IV, while the paper conclusion is presented in Section V.

II. RELATED WORKS

Different types of texture descriptors, such as LBP, LTP, and CLBC, are briefly discussed in this section. Despite the fact that the majority of these descriptors have a high classification accuracy, the researchers are currently exploring for additional distinct descriptors that may be employed for various computer vision tasks. In addition, the Redundant Discrete Wavelet Transform (RDWT) is briefly explained.

A. Local Binary Pattern (LBP)

The LBP is proposed by Ojala [15] for image texture classification. The LBP descriptor has been applied to various of applications, including dynamic texture recognition, face recognition, and shape localization. The basic of the LBP can be shown in Figure 3.

Thresholding and encoding are the two processes of the LBP. In the threshold stage, the value of the centre pixel in each pattern is compared to the value of its neighbour pixel to transform the results to a binary value (0 or 1). The goal of the thresholding phase is to acquire data on local binary differences. The following phase is the encoding process, in which the binary values obtained in the previous step are encoded and converted to a decimal value in order to characterise the pattern's structure.

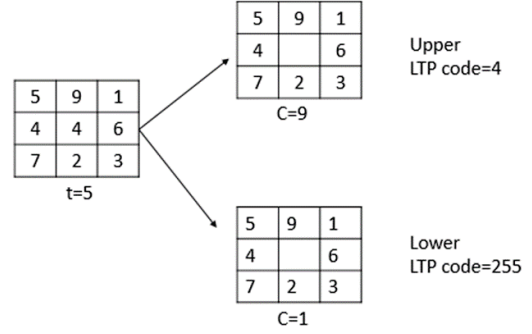


Fig. 4. The Local Ternary Pattern obtained with threshold =5

The LBP calculation can be mathematically described in Equation 1

$$LBP_{P,R} = \sum_{p=0}^{P-1} s(g_p - g_c)2^p, \quad s(x) = \begin{cases} 1, & x \geq 0 \\ 0, & x < 0 \end{cases} \quad (1)$$

Where radius R presents the grey value of the neighbour pixel on a circle and $g_p (p = 0, \dots, P-1)$ denotes the total number of the neighbours, g_c stands for the grey of the centre of pixels. Some of the neighbour's values around the centre can be estimated using bilinear interpolation.

B. Local Ternary Pattern (LTP)

The Local Ternary Pattern (LTP) is proposed to overcome the LBP sensitivity to noise drawback by [11]. The LTP is a variation of the LBP that uses three-valued codes (-1,0,1) to express variations between the centre and its neighbours, making it more noise-resistant. Figure 4 displays an example of the LTP operator. The mathematical expression of the LTP can be given as follows:

$$LTP_{P,R} = \sum_{p=0}^{P-1} s(g_p - g_c)2^p, \quad s(x) = \begin{cases} 1, & \text{if } x \geq t, \\ 0, & \text{if } -t < x < t, \\ -1, & \text{if } x < -t, \end{cases} \quad (2)$$

where t is a user specified threshold as shown in Figure 4.

C. Completed Local Binary Count (CLBC)

Zhao et al. suggested a new Local Binary Count (LBC) descriptor [13]. The number of value 1s in the binary neighbour group is only counted rather than coded in LBC. The number of 1s in the neighbour group in Figure 5 is 5, hence the local binary count code of the centre pixel is also 5.

$$LBC_{P,R} = \sum_{p=0}^{P-1} s(g_p - g_c), \quad s(x) = \begin{cases} 1, & \text{if } x \geq 0, \\ 0, & \text{if } x < 0, \end{cases} \quad (3)$$

The main difference between the LBC and the LBP is that the LBC just counts the amount of 1s in the local neighbour set, whereas the LBP uses the binary number to encode local patterns.

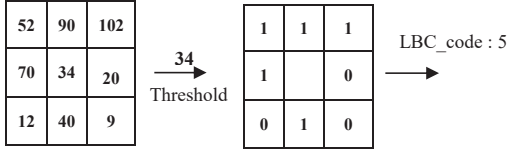


Fig. 5. LBC operator.

Zhao et al. [13] also extended the LBC to CLBC which is Completed Local Binary Count. It is same to CLBP have three operators which are Completed Local Binary Count_Centre (CLBC_C), Completed Local Binary Count_Magnitude (CLBC_M) and Completed Local Binary Count_Sign (CLBC_S). The CLBC_S is same as the original LBC as present in Equation 3.

The CLBC_S, CLBC_M and CLBC_C operators were also combined into joint or hybrid distributions and they were used for rotation invariant texture classification. The CLBC_M and CLBC_C can be described mathematically as follows:

$$CLBC_M_{P,R} = \sum_{p=0}^{P-1} s(m_p, c),$$

$$s(m_p, c) = \begin{cases} 1, & \text{if } |g_p - g_c| \geq c, \\ 0, & \text{if } |g_p - g_c| < c, \end{cases} \quad (4)$$

$$CLBC_C_{P,R} = s(g_c, c_I) \quad (5)$$

Where g_c and g_p are already defined in Equation 1, c is the average of m_p inside each pattern, and c_I is the image's average grey level. CLBC_M counts the number of neighbours with a significantly higher density than the centre pixel. As a result, it's used to get more information about the local intensity disparities.

D. Redundant Discrete Wavelet Transform (RDWT)

The Redundant Discrete Wavelet Transform (RDWT) is an estimate to the continued wavelet transform which takes out the downsampling operation from the discrete wavelet transform to create an over complete portrayal. Discrete wavelet transform has the move variation trademark which emerges from utilizing of down-examining operation, while RDWT is moving invariant where the spatial testing rate is settled crosswise over the scale.

As a result, each sub-group in the redundant discrete wavelet transform has the exact same size as the input information [16]. To address several previous wavelet transforms, Fowler *et al.* [17] presented the Redundant Discrete Wavelet Transform (RDWT). Unlike the discrete wavelet transform (DWT), which decomposes the image into four sub-bands with the same size as the original image, RDWT is shift invariant and decomposes the image into four sub-bands with the same size as the original image. Figure 6 depicts an example of the RDWT. As

a result, in each sub-band, the relevant textures in the image will be at the same spatial place. This results in a more precise capture of local texture and measurement of local texture.

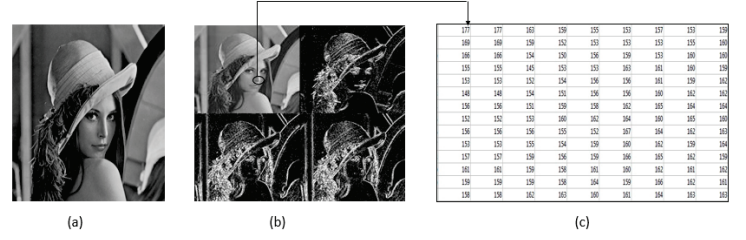


Fig. 6. a) an image b) RDWT c) pixel value of LL sub-band

III. PROPOSED WAVELET COMPLETED LOCAL TERNARY COUNT (WCLTC)

The proposed CLTC was extracted using the RDWT instead of the spatial domain (intensity pixel values) due to the RDWT's features. The CLTC is obtained by combining the LTP and CLBC descriptors. In this part, the WCLTC has explored in detail.

In $WCLTC_S$, local difference of the image is decomposed into two sign complementary components S_p^{upper} , S_p^{lower} . These components are used to build the $WCLTC_S_{P,R}^{upper}$, $WCLTC_S_{P,R}^{lower}$ respectively, as follows:

$$m_p^{upper} = |g_p - (g_c + t)|, \quad m_p^{lower} = |g_p - (g_c - t)| \quad (6)$$

$$s_p^{upper} = s(g_p - (g_c + t)), \quad s_p^{lower} = s(g_p - (g_c - t)) \quad (7)$$

$$WCLTC_S_{P,R}^{upper} = \sum_{p=0}^{P-1} s(g_p - (g_c + t)),$$

$$s_p^{upper} = \begin{cases} 1, & g_q \geq g_c + t \\ 0, & \text{otherwise} \end{cases} \quad (8)$$

$$WCLTC_S_{P,R}^{lower} = \sum_{p=0}^{P-1} s(g_p - (g_c - t)),$$

$$s_p^{lower} = \begin{cases} 1, & g_q \geq g_c - t \\ 0, & \text{otherwise} \end{cases} \quad (9)$$

Then $WCLTC_S_{P,R}$ is the concatenation of the $WCLTC_S_{P,R}^{upper}$ and $WCLTC_S_{P,R}^{lower}$, as follows:

$$WCLTC_S_{P,R} = [WCLTC_S_{P,R}^{lower} \quad WCLTC_S_{P,R}^{upper}] \quad (10)$$

where t denotes the user threshold while g_p , g_c defined in Equation 1.

In $WCLTC_M$, the local difference of the image is decomposed into two magnitude complementary components

m_p^{upper}, m_p^{lower} . These components are used to build the $WCLTC_{P,R}^{upper}$ and $WCLTC_{P,R}^{lower}$, respectively as described in the following equations.

$$WCLTC_{P,R}^{upper} = \sum_{p=0}^{P-1} t(m_p^{upper}, c),$$

$$t(m_p^{upper}, c) = \begin{cases} 1, & |g_p - (g_c + t)| \geq c \\ 0, & |g_p - (g_c + t)| < c \end{cases} \quad (11)$$

$$WCLTC_{P,R}^{lower} = \sum_{p=0}^{P-1} t(m_p^{lower}, c),$$

$$t(m_p^{lower}, c) = \begin{cases} 1, & |g_p - (g_c - t)| \geq c \\ 0, & |g_p - (g_c - t)| < c \end{cases} \quad (12)$$

$$WCLTC_{M_{P,R}} = [WCLTC_{P,R}^{lower} \quad WCLTC_{P,R}^{upper}] \quad (13)$$

Moreover, the $WCLTC_{P,R}^{upper}$ and $WCLTC_{P,R}^{lower}$ can be described mathematically as follows:

$$WCLTC_{P,R}^{upper} = t(c^{upper}, c_I) \quad (14)$$

$$WCLTC_{P,R}^{lower} = t(c^{lower}, c_I) \quad (15)$$

where c_I is mean value gray level of the whole image.

To generate the final histogram like the CLBC, the suggested WCLTC operators $WCLTC_S$, $WCLTC_M$, and $WCLTC_C$ are integrated into hybrid or joint distributions. The operators of the same type of pattern, i.e., the upper and lower pattern, are merged first into hybrid or joint distributions such as $WCLTC_{M/C}$, $WCLTC_{S/M/C}$, $WCLTC_{S/M}$, $WCLTC_{S/M/C}$. The findings are then combined to create the final operator histogram. Figure 7 summarises the WCLTC extraction procedure.

IV. EXPERIMENTS AND DISCUSSIONS

The proposed WCLTC is evaluated by a series of experiments on various texture and medical image datasets. The Outex database [18] and the Columbia-Utrecht Reflection and Texture (CURET) database [19] are two big and extensive texture databases used in these experiments. Furthermore, the performance of the proposed WCLTC descriptor is evaluated using three different medical image datasets: 2D Hela [20], VIRUS Texture [21], and BREAST CANCER (BR) dataset [22]. The proposed WCLTC is compared against CLBC [13], CLBP [12], and CLTP [14] in the experiments.

A. Dissimilarity Measuring Framework

Histogram intersection, log-likelihood ratio, and chi-square statistics are some of the methods for evaluating the dissimilarity between two histograms [6], [13]. The χ^2 statistics were utilised as a metric for dissimilarity in these experiments, with the nearest neighbourhood as the classifier. The χ^2

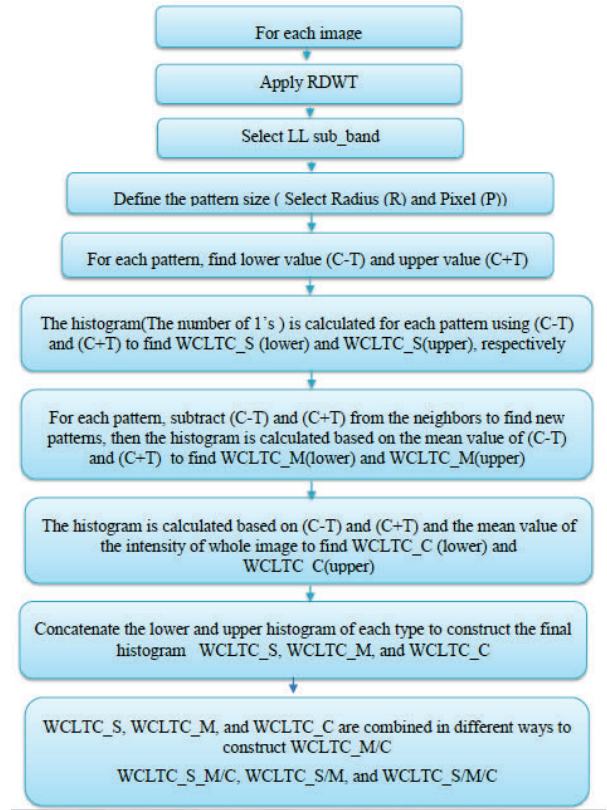


Fig. 7. The proposed WCLTC

distance between two histograms $H = h_i$ and $K = k_i$ where $(i = 1, 2, 3, \dots, B)$ can be mathematically described as follows:

$$Dissimilarity_{\chi^2}(H, K) = \sum_{i=1}^B \frac{(h_i - k_i)^2}{h_i + k_i} \quad (16)$$

B. Experimental Results on CURET Database

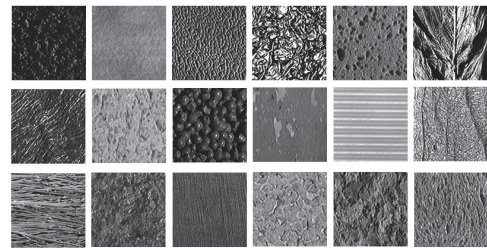


Fig. 8. Some images from CURET dataset.

A total of 61 texture classes are included in the CURET dataset [19]. Each class has 205 images that have been exposed to a variety of lighting and perspective situations. In each session, the images are captured from various angles. There are 118 image shots in each class with viewing angles smaller than 60° out of 250 total. Figure 8 shows some examples of CURET images. After converting to grayscale and trimming to 200×200 , only 92 images are chosen from these types of images. N images from 92 are used as training data in each

class, while the remaining images (92-N) are used as testing data. The average percentage of a hundred random splits is used to get the final classification accuracy. Table I shows the CURET average classification for $N = (6, 12, 23, 46)$.

The WCLTC performance is compared to the CLBC and the CLTP with different pattern sizes in Table I. With $WCLTC_S/M/C_{3,24}$, the proposed WCLTC achieved the maximum classification accuracy of 97.04%, while $CLBP_S/M/C_{3,24}$ achieved 95.72% and $CLTP_S/M/C_{3,24}$ reached 96.11%. Despite the fact that the $CLTP_S$, $CLTP_M$, and $CLTP_M/C$ outperformed the equivalent CLBC and WCLTC at all radiuses and in all N , the WCLTC outperformed the CLBC and CLTP.

C. Experimental Results on Outex Database

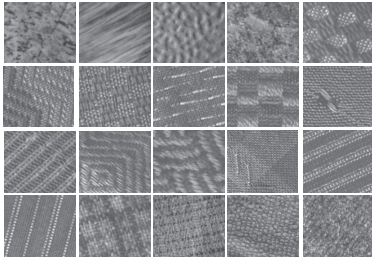


Fig. 9. Some images from Outex database.

There are 16 test suites in the Outex datasets, ranging from Outex TC 00010 (TC10) to Outex TC 00016 (TC16) [18]. These images were captured under various lighting, rotation, and scaling settings. The test suites Outex TC 00010 (TC10) and Outex TC 00012 (TC12) are well-known in the Outex databases. These two suites share the same 24 texture classes, which were gathered using three different illuminates ("horizon," "inca," and "t184") and nine different rotation angles (0° , 5° , 10° , 15° , 30° , 45° , 60° , 75° , and 90°). Each class has 20 non-overlapping texture samples with a size of 128×128 for each illumination and rotation circumstance. Figure 9 shows some examples of Outex images. 480 images are used as training data for TC10. These are images with "inca" illumination and a "0°" angle rotation. The images under the remaining rotation angles and "inca" illumination condition, i.e., 3840 images, are used as testing data. The training data for TC12 is the same as for TC10, but the testing data is all images taken under "t184" or "horizon" lighting circumstances, i.e. 4320 images for "t184" and 4320 images for "horizon." Table II shows the experimental results of TC10, TC12(t184), and TC12 (horizon). Figure 9 shows a few examples of Outex images.

Table II lists the experimental results of CLBP, CLBC, CLTP, and the proposed WCLTC. In TC10, the highest recognition accuracy was obtained by $CLTP_S/M/C_{3,24}$, which has reached up to 99.17% followed by the $WCLTC_S/M_{3,24}$, which has reached up 99.03%. In TC12, the proposed $WCLTC_S/M/C$ outperformed the $CLBP_S/M/C$, $CLBC_S/M/C$, and $CLTP_S/M/C$ in

both TC12(t184) and TC12(h). The best classification accuracy was obtained by $WCLTC_S/M/C_{3,24}$, which has reached up to 96.36% and 95.64% for TC12(t184) and TC12(h), respectively.

The experimental results of CLBP, CLBC, CLTP, and the proposed WCLTC are listed in Table II. The highest recognition accuracy in TC10 was achieved by $CLTP_S/M/C_{3,24}$, which achieved 99.17%, followed by $WCLTC_S/M_{3,24}$, which achieved 99.03%. In both TC12(t184) and TC12(h), the proposed $WCLTC_S/M/C$ outperformed the $CLBP_S/M/C$, $CLBC_S/M/C$, and $CLTP_S/M/C$. The best classification accuracy was achieved by $WCLTC_S/M/C_{3,24}$, which achieved 96.36% for TC12(t184) and 95.64% for TC12(h), respectively.

D. Experimental Results on 2D HeLa Database

DNA, Actin, Endosomes, ER, Golgi GPP130, Golgia, Lysosomes, Microtubules, Nucleolus, and Mitochondria are among the 10 classes in the 2D-HeLa database. Each class have a different number of images. 2D HeLa image examples can be found in Figure 10. In these experiments, 4/5 of images from each class are randomly chosen as training data and the rest 1/4 of images are used as testing data. The average percentage of 10 random splits is used to get the final classification accuracy. In these tests, the chi^2 -SVM classifier is utilised. In this experiment, the CLTP and WCLTC texture descriptors are used to analyse the 2D HeLa image database using three different texture patterns, as shown in Table III.

The WCLTC and CLTP texture operators are extracted using three different neighbour sizes ($P=8, 16, \text{ and } 24$) and three different texture pattern radius ($R = 1, 2, \text{ and } 3$). The categorization rate of CLTP and WCLTC descriptors is shown in table III. In several cases, the proposed WCLTC outscored the CLTP operators. The best classification accuracy was achieved by $WCLTC_S/M/C_{1,8}$, which achieved 96.91%, whereas the greatest classification accuracy was achieved by $CLTP_S/M_{2,16}$, which achieved 95.62%.

E. Experimental Results on Virus_Texture Database

The Virus Texture dataset is divided into 15 classes, each with 100 images. The CLTP and proposed WCLTC texture descriptors are used to analyse the Virus Texture image dataset in these experiments. 4/5 of images from each class are randomly chosen as training data, while the remaining 1/4 of images are used as testing data, similar to 2D-Hela. The average percentage of 10 random splits is used to get the final classification accuracy. In these tests, the chi^2 -SVM classifier is utilised. The WCLTC texture operators are extracted using three different neighbour sizes ($P=8, 16, \text{ and } 24$) and three different texture pattern radius ($R = 1, 2, \text{ and } 3$). Figure 11 shows some examples of Virus Texture images. Table IV displays the findings of the Virus Texture dataset. In general, the results are lower than expected, with $WCLTC_S/M/C_{3,24}$ achieving the highest classification accuracy of 72.44%. The highest classification accuracy was attained by $CLTP_S/M/C_{3,24}$, which was up to 71.56%.

TABLE I
CLASSIFICATION RATES % ON CURET DATABASE

	R=1, P=8				R=2, P=16				R=3, P=24			
	6	12	23	46	6	12	23	46	6	12	23	46
CLBC_S	56.88	66.21	72.89	78.82	63.49	72.68	79.49	85.35	60.82	70.57	74.21	80.14
CLTP_S	64.38	72.66	81.73	88.24	68.39	79.09	86.61	91.55	72.57	81.55	87.72	91.75
WCLTC_S	62.77	71.73	78.39	84.50	68.96	78.04	84.21	89.76	69.75	78.26	84.54	89.57
CLBC_M	50.12	58.62	57.82	66.61	58.57	68.28	76.11	83.03	51.23	60.53	68.36	77.41
CLTP_M	61.37	71.17	80.53	86.67	63.33	74.47	82.14	88.83	67.14	76.93	85.16	90.52
WCLTC_M	53.79	62.12	69.51	76.83	57.82	67.34	74.87	82.34	57.68	67.39	75.68	83.26
CLBC_M/C	56.53	67.15	75.58	82.97	64.81	75.56	82.98	89.75	68.71	78.54	86.04	91.65
CLTP_M/C	62.07	72.94	82.26	88.98	66.77	77.12	85.51	91.67	70.1	80.12	89.02	93.58
WCLTC_M/C	60.39	70.75	79.4	87.00	64.18	74.47	82.54	89.69	67.29	76.86	85.19	91.30
CLBC_S/M/C	66.63	76.54	85.02	90.55	70.27	80.47	87.57	92.78	73.29	82.28	89.28	94.07
CLTP_S/M/C	67.54	78.89	85.46	91.27	71.55	82.16	87.82	94.04	74.39	85.14	91.03	94.69
WCLTC_S/M/C	68.54	78.53	86.53	92.44	71.53	82.10	89.31	94.22	72.4	82.68	89.71	94.67
CLBC_S/M	69.89	79.88	86.62	93.1	74.63	83.44	89.67	93.85	74.95	84.3	90.83	94.53
CLTP_S/M	71.3	82.37	89.2	93.50	74.14	84.42	90.78	95.06	76.49	85.11	92.02	95.63
WCLTC_S/M	71.69	81.98	88.72	93.50	76.4	85.40	91.49	95.45	74.82	84.71	91.30	95.40
CLBC_S/M/C	72.85	82.95	90.12	94.78	76.07	85.73	92.15	95.67	76.8	86.54	92.00	95.72
CLTP_S/M/C	75.18	84.06	90.45	94.78	77.72	85.54	92.44	95.95	77.97	87.5	92.72	96.11
WCLTC_S/M/C	75.95	85.45	91.69	95.9	78.47	88.03	94.04	96.97	78.91	88.08	93.51	97.04

TABLE II
CLASSIFICATION RATES % ON OUTEX DATABASE

	R=1, P=8			R=2, P=16			R=3, P=24		
	TC10	TC12		TC10	TC12		TC10	TC12	
		T184	h		T184	h		T184	h
CLBP_S	84.41	65.46	63.68	89.40	82.26	75.20	95.07	85.04	80.78
CLBC_S	82.94	65.02	63.17	88.67	82.57	77.41	91.35	83.82	82.75
CLTP_S	94.14	75.88	73.96	96.95	90.16	86.94	98.20	93.59	89.42
WCLTC_S	89.97	80.30	78.24	95.65	92.61	92.61	98.04	93.28	91.45
CLBP_M	81.74	59.30	62.77	93.67	73.79	72.40	95.52	81.18	78.65
CLBC_M	78.96	53.63	58.01	92.45	70.35	72.64	91.85	75.59	74.58
CLTP_M	94.04	75.86	74.05	97.32	83.40	84.40	98.00	85.39	84.65
WCLTC_M	91.01	71.36	74.21	95.72	77.40	77.15	95.70	78.65	82.03
CLBP_M/C	90.36	72.38	76.66	97.44	86.94	90.97	98.02	90.74	90.69
CLTP_M/C	95.94	84.70	86.02	97.94	90.14	92.38	98.52	91.23	89.98
WCLTC_M/C	94.73	81.36	84.65	97.34	86.22	86.22	97.13	87.19	89.74
CLBP_S_M/C	94.53	81.87	82.52	98.02	90.99	91.08	98.33	94.05	92.40
CLTP_S_M/C	96.43	84.00	86.85	98.44	92.41	92.80	98.98	95.00	92.94
WCLTC_S_M/C	97.13	87.80	88.79	98.02	91.39	91.36	98.20	92.40	92.10
CLBP_S/M	94.66	82.75	83.14	97.89	90.55	91.11	99.32	93.58	93.35
CLBC_S/M	95.23	82.13	83.59	98.10	89.95	90.42	98.70	91.41	90.25
CLTP_S/M	96.41	82.85	84.81	97.84	92.06	92.69	99.04	94.14	92.59
WCLTC_S/M	96.90	85.85	86.66	98.56	92.17	92.71	99.03	93.65	92.10
CLBP_S/M/C	95.56	90.30	92.29	98.72	93.54	93.91	98.93	95.32	94.53
CLBC_S/M/C	97.16	89.79	92.92	98.54	93.26	94.07	98.78	94.00	93.24
CLTP_S/M/C	96.98	87.06	90.30	98.93	94.03	94.79	99.17	95.67	94.28
WCLTC_S/M/C	98.12	90.81	93.66	98.95	95.20	95.20	98.90	96.36	95.64

TABLE III
CLASSIFICATION RATES % ON 2D HELA DATABASE

	P=8,R=1	P=16,R=2	P=24,R=3
CLTP_S	84.57	91.98	93.21
WCLTC_S	88.89	90.74	93.20
CLTP_M	79.63	91.98	90.12
WCLTC_M	80.24	87.03	93.82
CLTP_M/C	89.51	90.12	90.12
WCLTC_M/C	91.97	93.20	93.20
CLTP_S/M/C	93.21	91.36	92.59
WCLTC_S/M/C	93.82	95.67	94.44
CLTP_S/M	94.44	95.62	91.98
WCLTC_S/M	96.29	95.67	95.67
CLTP_S/M/C	88.89	92.59	90.74
WCLTC_S/M/C	96.91	95.67	95.06

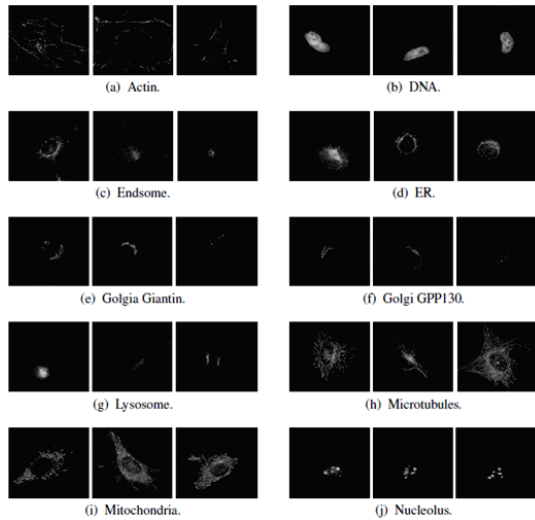


Fig. 10. Some images of 2D HeLa dataset.

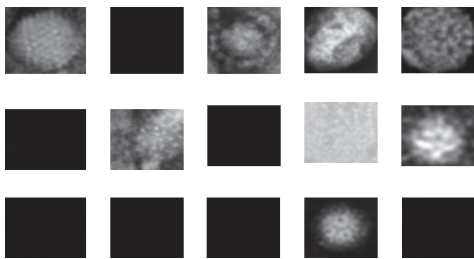


Fig. 11. Some images of Virus dataset_Texture

TABLE IV
CLASSIFICATION RATES % VIRUS-TEXTURE DATABASE

	P=8,R=1	P=16,R=2	P=24,R=3
CLTP_S	46.44	33.11	28.44
WCLTC_S	49.11	33.78	36.89
CLTP_M	52.67	52.11	26.88
WCLTC_M	52	51.78	59.78
CLTP_M/C	60.89	45.78	42.67
WCLTC_M/C	62.44	71.33	71.78
CLTP_S/M/C	66.44	51.56	48.44
WCLTC_S/M/C	65.11	69.78	72.89
CLTP_S/M	60.44	45.33	43.78
WCLTC_S/M	60	59.78	61.11
CLTP_S/M/C	71.56	50.22	45.11
WCLTC_S/M/C	70.67	70.44	72.44

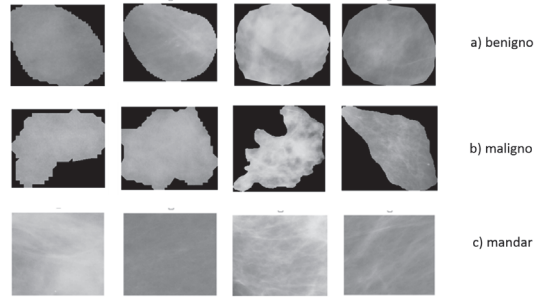


Fig. 12. Some images of BRdataset

F. Experimental Results on BR database

There are three classes in the BREAST CANCER (BR) database: benign cancer, control, and malignant cancer, with a total of 1394 images in those classes [22]. Figure 12 displays some examples of BR images. The proposed WCLTC and CLTP texture descriptors are used to analyse the BR image dataset in these experiments.

In these experiments, 4/5 of the images from each class are chosen at random as training data, while the remaining 1/4 are used for testing. The average percentage of 10 random splits is used to get the final classification accuracy. In these experiments, the *chi2*-SVM classifier is utilised. The WCLTC texture operators are extracted using three different neighbour sizes ($P=8, 16,$ and 24) and three different texture pattern radius ($R = 1, 2,$ and 3). The WCLTC performance for the BR dataset is shown in table V, where the CLTP outperformed the WCLTC in terms of classification accuracy utilising various texture patterns. The highest classification accuracy rate achieved by *CLTP_S/M*_{1,8} was 91.21%, while the best classification accuracy rate achieved by WCLTC was 89.69%, which was achieved by *WCLTC_S/M*_{2,16}.

The experiment findings reveal that the proposed WCLTC is able to achieve high classification rates with a variety of image datasets, including CURET, Outex, 2D-HeLa, and Virus Texture. Depending on the texture pattern radius, different

TABLE V
CLASSIFICATION RATES % ON BR DATABASE

	P=8,R=1	P=16,R=2	P=24,R=3
CLTP_S	83.53	83.36	84.71
WCLTC_S	86.9	87.5	88.17
CLTP_M	90.37	87.33	88.26
WCLTC_M	85.38	78.33	88
CLTP_M/C	90.11	89.86	88.85
WCLTC_M/C	86.31	88.68	89.1
CLTP_S_M/C	89.44	89.78	89.52
WCLTC_S_M/C	88.26	88.93	89.69
CLTP_S/M	91.21	89.1	89.02
WCLTC_S/M	86.9	88.68	89.35
CLTP_S/M/C	90.03	90.7	89.94
WCLTC_S/M/C	88.68	88.76	89.02

results were obtained. This is due to the information's location within each dataset class's images. In some datasets, wavelet information performed much better than the spatial domain in terms of classification accuracy.

V. CONCLUSION

The WCLTC texture descriptor was presented as a new discriminative texture descriptor that combines the LTP and CLBC descriptors. The limitations of both LTP and CLBC acquired from the original LBP are overcome by this integration. The proposed descriptor was called Completed Local Ternary Count (CLTC). Furthermore, the proposed CLTC was enhanced to improve its discriminative property by extracting it using wavelet coefficients, which is RDWT. Two types of texture databases, CURET and Outex, as well as three medical datasets, 2D HeLa, Virus Texture, and BR, were used to evaluate the performance of the proposed WCLTC. In both texture and medical image experiments, the WCLTC demonstrated good classification accuracy. Some prior texture descriptors, such as CLTP, CLBC, and CLBP, performed worse than the WCLTC. With the 2D HeLa, CURET, and Virus datasets, the WCLTC achieved the highest classification accuracy of 96.91%, 97.04%, and 72.89%, respectively.

ACKNOWLEDGMENT

This work was supported by Universiti Malaysia Pahang through the Research Grant Scheme (FRGS), Ministry of Higher Education, Grant RDU190173 and University Malaysia Pahang Grant RDU190333.

REFERENCES

[1] J. Xiao, J. Hays, K. A. Ehinger, A. Oliva, and A. Torralba, "SUN database: Large-scale scene recognition from abbey to zoo," in *Computer vision and pattern recognition (CVPR), 2010 IEEE conference on*. IEEE, 2010, pp. 3485–3492.

[2] A. Moh'd Shamaileh, T. H. Rassem, L. S. Chuin, and O. N. Al Sayaydeh, "A new feature-based wavelet completed local ternary pattern (Feat-WCLTP) for texture image classification," *IEEE Access*, vol. 8, pp. 28 276–28 288, 2020.

[3] K. M. Alalayah, R. R. Irshad, T. H. Rassem, and B. A. Mohammed, "A new fast local laplacian completed local ternary count (FLL-CLTC) for facial image classification," *IEEE Access*, vol. 8, pp. 98 244–98 254, 2020.

[4] S. Y. Yee, T. H. Rassem, M. F. Mohammed, and S. Awang, "Face recognition using laplacian completed local ternary pattern (LapCLTP)," in *Advances in Electronics Engineering*. Springer, 2020, pp. 315–327.

[5] X. Wang, T. X. Han, and S. Yan, "An hog-lbp human detector with partial occlusion handling," in *Computer Vision, 2009 IEEE 12th International Conference on*. IEEE, 2009, pp. 32–39.

[6] T. H. Rassem, M. F. Mohammed, B. E. Khoo, and N. M. Makbol, "Performance evaluation of completed local ternary patterns (CLTP) for medical, scene and event image categorisation," in *Software Engineering and Computer Systems (ICSECS), 2015 4th International Conference on*. IEEE, 2015, pp. 33–38.

[7] R. L. Kashyap and A. Khotanzad, "A model-based method for rotation invariant texture classification," *IEEE Transactions on Pattern Analysis and Machine Intelligence*, no. 4, pp. 472–481, 1986.

[8] J. Duvernoy, "Optical-digital processing of directional terrain textures under translation, rotation, and change of scale," *Applied optics*, vol. 23, no. 6, pp. 828–837, 1984.

[9] T. Ojala, M. Pietikainen, and T. Maenpaa, "Multiresolution gray-scale and rotation invariant texture classification with local binary patterns," *IEEE Transactions on pattern analysis and machine intelligence*, vol. 24, no. 7, pp. 971–987, 2002.

[10] V. Takala and M. Pietikainen, "Multi-object tracking using color, texture and motion," in *Computer Vision and Pattern Recognition, 2007. CVPR'07. IEEE Conference on*. IEEE, 2007, pp. 1–7.

[11] X. Tan and B. Triggs, "Enhanced local texture feature sets for face recognition under difficult lighting conditions," *IEEE transactions on image processing*, vol. 19, no. 6, pp. 1635–1650, 2010.

[12] Z. Guo, L. Zhang, and D. Zhang, "A completed modeling of local binary pattern operator for texture classification," *IEEE Transactions on Image Processing*, vol. 19, no. 6, pp. 1657–1663, 2010.

[13] Y. Zhao, D.-S. Huang, and W. Jia, "Completed local binary count for rotation invariant texture classification," *IEEE transactions on image processing*, vol. 21, no. 10, pp. 4492–4497, 2012.

[14] T. H. Rassem and B. E. Khoo, "Completed local ternary pattern for rotation invariant texture classification," *The Scientific World Journal*, vol. 2014, 2014.

[15] T. Ojala, M. Pietikainen, and D. Harwood, "A comparative study of texture measures with classification based on featured distributions," *Pattern recognition*, vol. 29, no. 1, pp. 51–59, 1996.

[16] C. Cortes and V. Vapnik, "Support-vector networks," *Machine learning*, vol. 20, no. 3, pp. 273–297, 1995.

[17] J. Fowler, "The redundant discrete wavelet transform and additive noise," *IEEE Signal Process Lett*, vol. 12, no. 9, pp. 629–632, sept. 2005.

[18] T. Ojala, T. Maenpaa, M. Pietikainen, J. Viertola, J. Kyllonen, and S. Huovinen, "Outex-new framework for empirical evaluation of texture analysis algorithms," in *Pattern Recognition, 2002. Proceedings. 16th International Conference on*, vol. 1. IEEE, 2002, pp. 701–706.

[19] M. Varma and A. Zisserman, "Classifying images of materials: Achieving viewpoint and illumination independence," in *Proceedings of 7th European Conference on Computer Vision*, vol. 3, May 2002, pp. 255–271.

[20] M. V. Boland and R. F. Murphy, "A neural network classifier capable of recognizing the patterns of all major subcellular structures in fluorescence microscope images of hela cells," *Bioinformatics*, vol. 17, no. 12, pp. 1213–1223, 2001.

[21] G. Kylberg, M. Uppström, K.-O. Hedlund, G. Borgefors, and I.-M. SINTORN, "Segmentation of virus particle candidates in transmission electron microscopy images," *Journal of microscopy*, vol. 245, no. 2, pp. 140–147, 2012.

[22] G. B. Junior, A. C. de Paiva, A. C. Silva, and A. C. M. de Oliveira, "Classification of breast tissues using moran's index and geary's coefficient as texture signatures and svm," *Computers in Biology and Medicine*, vol. 39, no. 12, pp. 1063–1072, 2009.